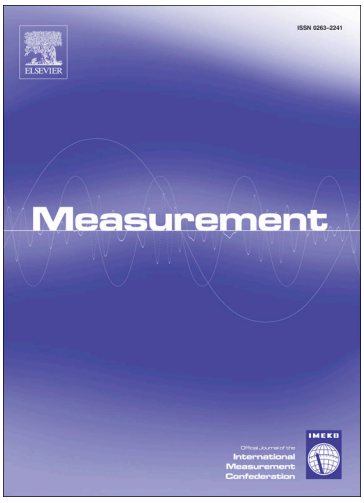

The 88-Inch Cyclotron: A One-Stop Facility for Electronics Radiation and Detector Testing

M. Kireeff Covo, R.A. Albright, B.F. Ninemire, M.B. Johnson, A. Hodgkinson, T. Loew, J.Y. Benitez, D.S. Todd, D.Z. Xie, T. Perry, L. Phair, L.A. Bernsteiny, J. Bevins, J.A. Brown, B.L. Goldblum, M. Harasty, K.P. Harrig, T.A. Laplace, E.F. Matthews, A. Bushmaker, D. Walker, V. Oklejas, A.R. Hopkins, D.L. Bleuel, J. Chen, S.B. Cronin

PII: S0263-2241(17)30640-1
DOI: https://doi.org/10.1016/j.measurement.2017.10.018
Reference: MEASUR 5020

To appear in: *Measurement*

Received Date: 31 August 2017
Accepted Date: 9 October 2017

Please cite this article as: M. Kireeff Covo, R.A. Albright, B.F. Ninemire, M.B. Johnson, A. Hodgkinson, T. Loew, J.Y. Benitez, D.S. Todd, D.Z. Xie, T. Perry, L. Phair, L.A. Bernsteiny, J. Bevins, J.A. Brown, B.L. Goldblum, M. Harasty, K.P. Harrig, T.A. Laplace, E.F. Matthews, A. Bushmaker, D. Walker, V. Oklejas, A.R. Hopkins, D.L. Bleuel, J. Chen, S.B. Cronin, The 88-Inch Cyclotron: A One-Stop Facility for Electronics Radiation and Detector Testing, *Measurement* (2017), doi: https://doi.org/10.1016/j.measurement.2017.10.018

The 88-Inch Cyclotron: A One-Stop Facility for Electronics Radiation and Detector Testing

M. Kireeff Covo*, R. A. Albright, B. F. Ninemire, M. B. Johnson, A. Hodgkinson, T. Loew, J. Y. Benitez, D. S. Todd, D. Z. Xie, T. Perry, and L. Phair
[†]88- Inch Cyclotron
Lawrence Berkeley National Laboratory
1 Cyclotron Road, Berkeley, California 94720, USA
*mkireeffcovo@lbl.gov

L.A. Bernsteiny[†], J. Bevins, J.A. Brown, B.L. Goldblum, M. Harasty, K.P. Harrig, T. A. Laplace, E.F. Matthews
Department of Nuclear Engineering,
University of California,
4155 Etcheverry Hall, MC 1730, Berkeley, California 94720, USA

A. Bushmaker, D. Walker, V. Oklejas, and A. R. Hopkins
Physical Sciences Laboratories
The Aerospace Corporation
355 S. Douglas Street, El Segundo, California 90245, USA.

D. L. Bleuel
Lawrence Livermore National Laboratory,
Livermore, California 94550, USA

J. Chen and S. B. Cronin
The University of Southern California
Los Angeles, CA 90089

***Abstract*— In outer space down to the altitudes routinely flown by larger aircrafts, radiation can pose serious issues for microelectronics circuits. The 88-Inch Cyclotron at Lawrence Berkeley National Laboratory is a sector-focused cyclotron and home of the Berkeley Accelerator Space Effects Facility, where the effects of energetic particles on sensitive microelectronics are studied with the goal of designing electronic systems for the space community. This paper describes the flexibility of the facility and its capabilities for testing the bombardment of electronics by heavy ions, light ions, and neutrons. Experimental capabilities for the generation of neutron beams from deuteron breakups and radiation testing of carbon nanotube field effect transistor will be discussed.**

Keywords—Radiation Hardening; Single Event Effects; Ion Beam; Neutron Beam; Cyclotron; ECR

I. Introduction

The atmosphere and the Earth's magnetic field shield the planet's surface from most of the ionizing radiation that originates from the Sun and other stars.

The solar wind boils continuously off the Sun and is constituted of 80% protons, 18% alpha particles, and traces of heavier charged particles [1]. It has a similar composition to the galactic cosmic rays that originate outside the solar system. Occasionally, however, a magnetic disturbance in the Sun results in an explosive ejection of huge amounts of matter from the solar corona, known as coronal mass ejection, which can be responsible for showers of high energy particles impacting Earth's atmosphere within 15-20 minutes of the event [2].

The first spacecrafts lost due to total radiation dose effects occurred unexpectedly in 1962. Telstar and six other satellites were lost within a seven-month period after a high altitude nuclear weapon test produced a large number of beta particles, which caused a new and very intense radiation belt lasting until the early 1970s [3].

When high-energy ions enter a material, they lose energy to the medium. The energy loss from the projectile per unit path length is known as stopping power, which has nuclear and electronic components.

The nuclear stopping power is caused by elastic collisions with the nuclei of the target material. The electronic stopping power is produced by inelastic collisions with the electrons [4]. Electronic stopping power is equivalent to the linear energy transfer (LET) for the ions produced by the cyclotron.

The energy deposited from the electronic stopping power produces a dense track of electron-hole pairs along the ion track by the ionization process. If the ion interacts with an electronic semiconductor component, some charge will be collected at the p-n junction, while others will recombine [5]. As a result, a very short duration current pulse is generated at the circuit node, which can produce transient effects such as single-event upset and multiple-bit upset, catastrophic events with single-event latch-up and snapback, and single-event hard errors [6]. Long term material degradation may be produced by rapid charge collection, annealing, or by displacement damage caused by elastic collisions with lattice nuclei.

The 88-Inch Cyclotron was supported by the Director, Office of Science, Office of Nuclear Physics, Division of Nuclear Physics, U.S. Department of Energy under Contract No. DE-AC02-05CH11231. The Bay area Neutron Group was supported by the Department of Energy National Nuclear Security Administration through the Nuclear Science and Security Consortium under Award Numbers DE-NA-0003180 and DE-NA-0000979. The University of Southern California was supported by the Department of Energy DOE Award No. DE-FG02-07ER46376 (J.C.) and NSF Award No. 1402906 (S.C.). The Aerospace Corporation was funded by the Independent Research and Development program. The UCSB nanofabrication facility is part of the NSF and was funded by the NNIN network. Sample fabrication was supported by the U.S. Department of Energy, Office of Basic Energy Sciences, Division of Materials Sciences and Engineering under Contract No. DE-FG02-07ER46376.

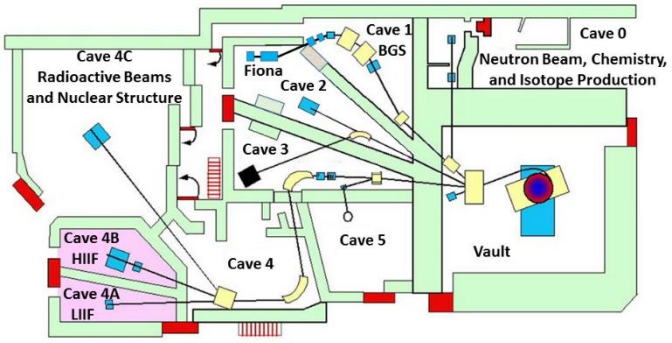

Fig. 1. Layout of the 88-Inch Cyclotron Facility.

Knowledge of the mechanisms underlying the radiation response of electronic devices is of paramount importance for devising hardness assurance methodologies to test device reliability, and developing radiation hardened circuits and design techniques to improve the tolerance of electronic circuits to specific effects of radiation.

Ions traversing a material have the property of depositing most of the energy immediately before coming to rest, i.e. at the Bragg peak. This allows ions to be used to probe isolated parts of electronic devices.

As the loss of a piece of equipment in space can be very costly, scientists and engineers from the aerospace industry, NASA and the Department of Defense perform radiation effects studies using accelerators and other facilities.

This paper discusses the capabilities of the 88-Inch Cyclotron at Lawrence Berkeley National Laboratory, which is the home of the Berkeley Accelerator Space Effects (BASE) Facility, to provide well-characterized beams of neutrons, heavy ions, and light ions that simulate the space environment [7].

II. 88-Inch Cyclotron

The cyclotron has five experimental caves, as shown in Fig. 1. Cave 0 research is mainly for neutron beam, chemistry, and isotope production. Cave 4A and 4B, part of the Berkeley Accelerator Space Effects (BASE), are a Light-Ion Irradiation Facility (LIIF) and Heavy-Ion Irradiation Facility (HIIF), respectively. Cave 4C is used for radioactive beams and nuclear structure experiments and it is the cave where the world's most sensitive gamma-ray detector, GRETINA [18], was commissioned. Cave 1 has the Berkeley Gas-filled Separator (BGS) used for chemistry and physics research of the super heavy elements [19]. The by-products of BGS go to a recently commissioned gas catcher, RF quadrupoles, and an acceleration region before entering Cave 2 and reaching the Facility for Identification of Nuclide A (FIONA) isotope separator [20]. Caves 3, 4, and 5 currently do not have any ongoing experiments.

A. *Electron Cyclotron Resonance Ions Sources*

The cyclotron has three ion sources that have led to progressively higher intensities and charge states of heavier ions, Fig. 2. The first generation of electron cyclotron resonance (ECR) ion source was coupled to the cyclotron in the early 1980s. It has a 6.4 GHz Klystron that generates 2.5 kW of power and provides the primary heating frequency. In conventional ECR sources [8], the ECR zones are usually thin annular, ellipsoidal-shaped surfaces which surround the optical axis of the source. The ECR magnetic field for confinement is less than 0.4 T.

Geller's scaling law [9] predicts that the density of the plasma is directly proportional to the RF frequency squared, so it encourages to increase the frequency with the consequent rise of the magnetic field.

The second generation, the Advanced ECR - Upgrade ion source (AECR-U), was built and upgraded in the 1990s with maximum confinement magnetic field of 1.7 T [10]. It has one 14 GHz Klystron that generates 2.5 kW of power and provides the primary heating frequency and a 10.75 to 12.75 GHz Traveling-Wave Tube (TWT) amplifier that generates 400 W of RF power and provides the secondary heating frequency. The TWT, installed in 2010, replaced a Klystron amplifier with the goal of further optimizing the source performance [11].

The third generation, the superconducting ECR source named Versatile Ecr ion source for Nuclear Science (VENUS), was operational in early 2000s [12]. It has a 28 GHz Gyrotron that provides 10 kW of power for the primary heating frequency, and a 18 GHz Klystron that provides 2.5 kW of power for the secondary heating frequency. VENUS is the first ECR to reach a maximum magnetic field strength of 4 T and it has produced a great number of record intensity of medium and high charge state heavy ion beams, which places it among the most powerful superconducting ECR ion source worldwide.

The feasibility study and preliminary development to build a fourth generation ECR ion source, called Mixed Axial and Radial field System - Demonstration (MARS-D), are underway. The operating frequency will be up to 45 GHz with a magnetic confinement field of 6T [13] and is expected to further enhance the capability of the 88-Inch Cyclotron.

B. *"Cocktail" of Ions*

Ions produced by ECR ion sources are injected inside the

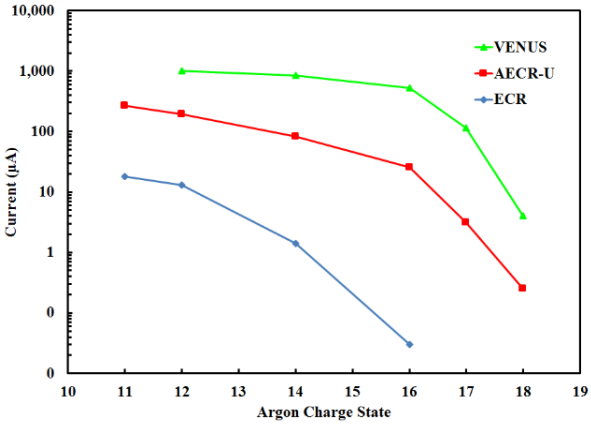

Fig. 2. Argon current versus charge state produced by ECR, AECR-U, and VENUS sources.

88-Inch Cyclotron. After the ions enter the cyclotron, they are accelerated by a radiofrequency (RF) electric field and held to a spiral trajectory by a static magnetic field. The RF fields cause the ions to bunch up into packets. The ions gain velocity and the orbit increases with radius. The ions that are not synchronized with the RF are lost.

The cyclotron operates in the frequency range of 5.5 to 16.5 MHz, but it can operate using harmonic acceleration, so the energy range of the machine is limited only by the capabilities of the magnet, not the RF system.

During the cyclotron operation, ions of near identical mass-to-charge ratio are tuned out of the source simultaneously and adjustments of the cyclotron frequency can separate them with a mass resolution of 1/3000 [14]. Therefore, the combination of cyclotron and ECR sources provide the unique ability to run "cocktails" of ions. A cocktail is a mixture of ions of near-identical charge-to-mass ratio [15]. The current heavy ion cocktails available are the 4.5, 10, 16, and 30 MeV/u.

The wideband driven RF system for the cyclotron provides fast beam tuning, allowing users to switch back and forth between several ion species of the same cocktail with small frequency adjustments, so a new beam does not require retuning the whole accelerator and is accomplished in approximately one minute.

The cyclotron provides different ion species and charge states for energy variable experiments, which take advantage of the different stopping power and range of ions into the components under examination.

To improve the cyclotron efficiency and allow high-current experiments, the innermost trim coils 1 and 15 were modified in 2013-14 to provide a current imbalance and alter the center region magnetic field strength, producing a magnetic mirror effect that offsets and displaces the beam axially [16].

A nondestructive beam current monitor, mounted after the deflectors and commissioned in 2014, can concurrently monitor the beam current delivered. It has exceptional resolution, long term stability, and can measure the beam current extracted from the cyclotron as low as 1 nA [17].

III. Radiation Testing Capabilities

A. BASE Facility

The layout of the 88-Inch Cyclotron Facility, Fig. 1, shows the BASE Facility at the shaded lower left side.

1) Heavy-Ion Irradiation Facility (HIIF)

The HIIF testing takes place in the vacuum chamber located in Cave 4B. Four heavy ion cocktails regularly available (4.5, 10, 16 and 30 AmeV) are summarized in 0Depending on the cocktail, LETs from 1 to 100 MeV/mg/cm^2, range from 40 µm to 1400 µm, and flux levels of up to 10^7 ions/cm^2/sec are available.

To tune the beam into the cave, the beam is first evenly spread out to a circle of 5 cm diameter on the cave phosphor and viewed with a digital camera. Then the beam is attenuated and five Hamamatsu R647 photomultiplier tubes (PMTs) are inserted. Four PMTs are placed around the edge of the beam, and one is placed in the middle. These PMTs are then calibrated against the current, after which the center PMT is removed to permit exposure of the target.

The PMT signal is then sent up to a data acquisition system. The beam may be stopped manually or by setting run time, fluence, or effective fluence limits.

Parts tested can be remotely positioned horizontally, vertically, or rotationally with a motion table inside the vacuum chamber. An alignment laser is available to ensure the part is in the center of the beam.

2) Light-Ion Irradiation Facility (LIIF)

The LIIF is located in Cave 4A and it is set up to run samples in air. Beam particles are tuned to a 10 cm diameter and travel through a nitrogen-filled ion chamber, where they leave a trail of electrons that are collected by four quadrant concentric electrodes with diameters of 1, 2, 4, 6, and 8 cm. After the beam has achieved proper uniformity, a collimator with diameters of 2.5, 5, 7.5, or 10 cm is placed on the ion chamber and an exposure is made with Gafchromic film and scanned.

The final processing and indication of ion chamber data provides the user with flux and fluence values for each ring and quadrant, so fluence limits can be set to stop the beam upon reaching a threshold level.

The LIIF is capable of providing standard fluxes of up to 10^9 protons/cm^2/sec. Standard proton energies include 13.5, 20, 30, 40, 50, and 55 MeV, but it can be used with other light-ions and the light-ion cocktail. The energy loss in the ion chamber and air limits the lower energy running in this facility. If the experiment requires, lower energy protons can be run in the vacuum chamber located in cave 4B.

B. Neutron Beams

In the cave 0 beamline, a deuteron beam hits a beryllium or tantalum thin target and splits up into a proton and neutron [21], because deuterons have a low binding energy of 2.22 MeV.

This process yields a tunable forward focused quasi-monoenergetic neutron beams that are available with tunable energies that range of from 8 to 30 MeV and fluxes of up to 10^8 neutrons/cm^2/sec.

The beryllium target provides a higher yield neutron beam and the tantalum target produces a lower yield to cave 01/02. The absolute flux can be measured at the target station using standard activation foil techniques.

The energy distributions can be measured directly using time-of-flight (TOF) techniques and neutron activation and pulse height spectrum unfolding methods [22].

Microampere-level energetic deuteron beams also can be used to form intense, broad-spectrum neutron beams for use in a host of basic and applied nuclear science activities. The neutrons are produced via the thick target deuteron break-up (TTDB) mechanism that has been studied in the past by

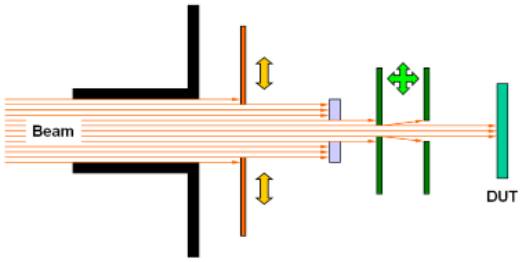

Fig. 4. Milli-Beam Schematic. The arrows show the possible motion of the different collimators.

Schweimer [23] and Meulders [24]. The TTDB mechanism involves a combination of nuclear and Coulombic break-up of the deuteron beam as it traverses a thick target. While the average energy of the neutrons from TTDB is approximately half of the incident beam energy less the deuteron binding energy, the fact that the beam is slowing as it traverses a thick target gives rise to a relatively broad energy spectrum whose end point is at the beam-energy plus the reaction Q-value. The TTDB mechanism is an efficient way to generate fast neutrons, particularly if a low-Z break-up target such as carbon or beryllium is used where up to 10% of the beam can be converted into neutrons at forward angles.

Fig. 3 shows the layout of the TTDB neutron beam at the cave. High-current energetic deuteron beams are sent through a switching magnet and a bending magnet and made incident on a water-cooled breakup target in the vault. The resulting forward-focused neutron beam travels through the wall separating the vault from Cave 01 where its energy can be determined using the time-of-flight (TOF) approach or by unfolding the measured pulse height spectrum. This mechanism has already been used by researchers at UCB, LBNL and LLNL to determine the temporal characteristics and light-yield for novel neutron scintillating materials [25]. Given that the cyclotron has multi-turn extraction, the train of bunches width cannot be adjusted below few hundred nanoseconds. An effort to produce a single turn extraction is underway to space the bunches to avoid the "wrap around" effect, where slow neutrons from the previous bunch superimpose fast neutrons from the present bunch, allowing unambiguous measurement of the neutron energy via TOF. If the deuteron beam is made incident on a breakup target in Cave 01, wide-spectrum neutron damage studies can be carried out where displacement-driven damage can be carried out at an exceptional accelerated rate as compared to a nuclear reactor core.

In addition, the TTDB neutron beam is being used by the LBNL/UC Nuclear Data Group to perform (n,n'γ) measurements to improve neutron transport simulations and to probe the properties of highly-excited nuclear states below of the neutron separation energy. Similar measurements are taking place at HZDR [26] and GELINA [27].

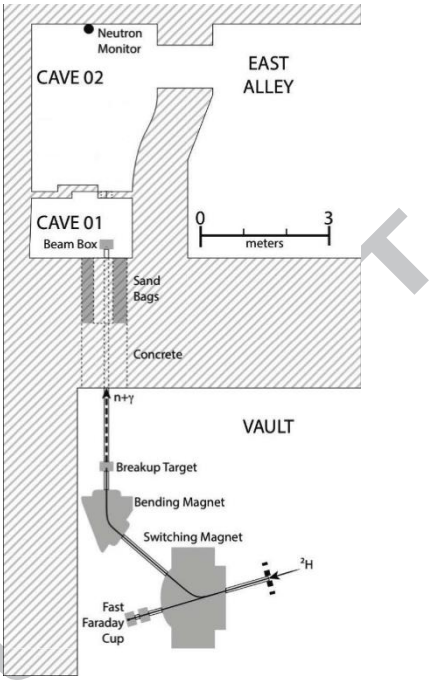

Fig. 3. Schematic of the thick target deuteron breakup neutron source in Cave 0 at the LBNL 88-Inch Cyclotron

C. Microbeam

As semiconductor parts become more miniaturized, new modes of failure appear and experimenters not only need to test whole components, but also to isolate and probe small sections of the electronics from the device under test (DUT) to pinpoint problems. Furthermore, accelerators can be used to produce pencil beams for studying the basic mechanisms contributing to single event effects (SEE).

The 88-Inch Cyclotron is unique in producing parallel beams. A series of collimators with precision slits, located inside cave 4B, produce a Milli-Beam for SEE characterization [28], shown in Fig. 4. The advanced test sub-system provides SEE spatial error isolation of approximately 10 to 30 µm minimum and up to 100 to 300 µm maximum, depending on the desired scan rate.

IV. Experimental Measurements

A. Neutron Spectrum from 16 MeV Deuteron Breakup

Fig. 5 shows a set of representative neutron beam spectra from the TTDB for a 20 µA 16 MeV deuteron on beryllium (LBNL 16 MeV on Be) and a 33 MeV deuteron on tantalum (LBNL 33 MeV on Ta) with error bars included together with a similar measurement by Meulders for a 33 MeV deuteron on beryllium (Meuders 33 MeV on Be) [24]. Also plotted is the spectrum from the Weapons Neutron Research Facility at Los Alamos National Laboratory (WNR-15L) assuming a beam current of 4 µA and a 6% duty cycle.

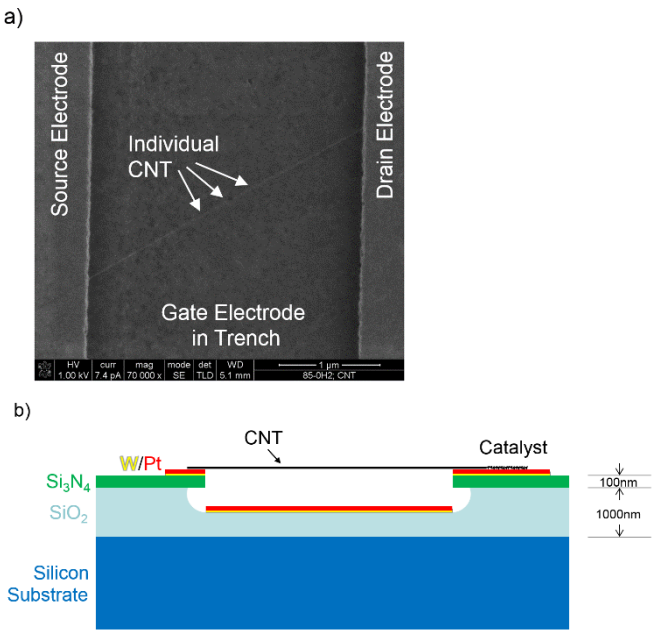

Fig. 6. Suspended carbon nanotube field effect transistor. (a) Scanning electron microscope image. (b) Schematic representation. Suspended portion is 500 nm to 2 µm in length, with 500 nm of air between the gate and CNT.

For the LBNL 16 +Be and 33 MeV +Ta TTDB measurements, neutrons were detected using an EJ-309 organic scintillator coupled to a Hamamatsu H1949-50 photomultiplier tube at 683.78 cm and 686.4 cm from the breakup target, respectively. For the LBNL 16 MeV +Be, pulse height and pulse shape data were obtained using the mesytec MPD-4 modules as fast variable gain input amplifiers fed to a CAEN V785 peak sensing analog-to-digital converter (ADC). Data were acquired for a period of 48.8 minutes and recorded using the MIDAS data acquisition system [29]. Data reduction was performed using the ROOT data analysis framework [30]. For the LBNL 33 MeV +Ta, signals were read using a 500 MHz, 14-bit digitizer (CAEN V1730) with on-board pulse shape discrimination and digital pulse shaping. Data were acquired for a period of 921 seconds and recorded using CAEN DPP-PSD control software.

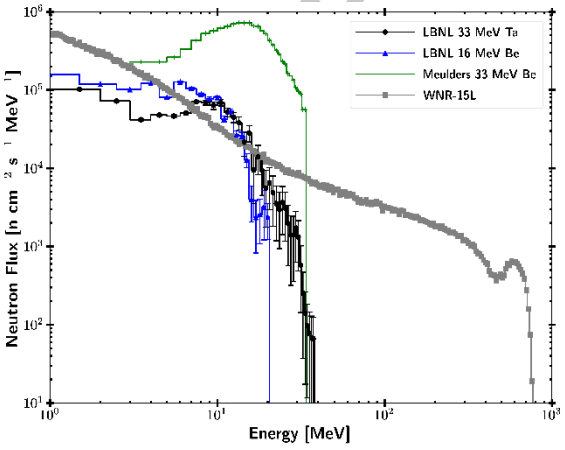

Fig. 5. Comparison between the neutron spectrum in Cave 0 at the LBNL 88-Inch Cyclotron from 16 MeV deuteron breakup on Be, 33 MeV breakup on Ta and 33 MeV breakup on Be from an earlier work by Meulders is plotted as well as the spectrum at the 15L beamlines at LANSCE/WNR.

The neutron spectra were obtained using pulse height spectrum unfolding via the GRAVEL and MIEKE sequence from the HEPROW package [31]. The characteristic response matrix of the EJ-309 detector was simulated using an experimentally-benchmarked GEANT4 simulation and smeared with a measured resolution function [32, 33]. The unfolded spectrum was normalized using the beam current measured at the Faraday cup on the breakup target in cyclotron vault.

The TTDB neutron beam in Cave 0 is remarkably intense and well suited to a wide variety of nuclear science and engineering experiments. The comparison between the LBNL and WNR sources in Fig. 5 highlights valuable aspects of the neutron beam at the cyclotron.

While both neutron sources have a broad energy spectrum, the 88-Inch Cyclotron neutron source can be "tuned" to cover a wider or narrower energy range.

The LANSCE/WNR source includes neutrons up to the incident proton beam energy of 800 MeV, whereas the vast majority of neutron nuclear science and engineering applications are centered below 20 MeV. These higher energy neutrons can be a troublesome feature in some applications, leading to complications in determining instrument response and rendering activation-based flux measurement impossible to perform.

This combination of characteristics makes the TTDB neutron source at LBNL well-suited for a wide range of nuclear science and engineering applications ranging from (n,x) cross section measurements to neutron damage studies to detector characterization [34].

B. Radiation Testing of Carbon Nanotube Field Effect Transistor

Progress in device-level research has matured carbon nanotube field effect transistors (CNT FETs), and they are now being considered as a promising new technology for next-generation micro- and nano-electronic devices and circuitry because of the potential performance advantages and novel properties available [35-40]. Single-walled CNTs also provide an excellent system for studying one-dimensional physics [41-48].

As nanoelectronic devices are scaled to smaller node sizes and incorporate alternative device structures, radiation effects studies are needed to understand the effects of these changes on device performance in radiation environments such as in space or particle accelerators. Several important radiation studies on CNT based field effect transistor (FET) devices have shown marginal to minimal [49-52] sensitivity to total ionizing
dose (TID) effects. In general, scaling has resulted in some mitigation of TID effects in all nanoelectronic devices, and conversely, an increase in sensitivity to SEE, caused by the lower capacitance of individual nodes in microelectronics and

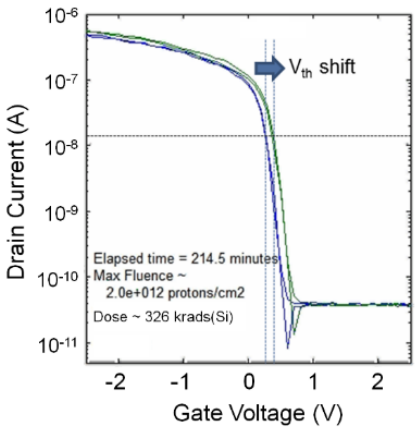

Fig. 8. Drain current versus gate voltage before (blue) and after (green) exposure to 2x1012 protons/cm2. The corresponding dose is 326 krads(Si). A small threshold voltage shift of less than 200 mV is observed.

higher sensitivity to charge deposition and transport.

As electronic devices are scaled further toward the one-dimensional channel limit, fluctuations in charge and bonding configuration of defects and traps near the channel have become increasingly important, even at the single electron level. This has been seen in CNTs [53-56], in molecular electronic systems [57], and also as random telegraph noise in scaled silicon devices [58-60]. When the root cause for these events involves radiation, they are generically referred as transient radiation events (TREs).

In this study, isolated, suspended, single-walled carbon nanotube FETs were electrically probed in-situ during exposure to proton radiation fluxes. Threshold voltage shifts and large changes in resistance by up to two orders of magnitude were observed, which are attributed to one-at-a-time adsorption of radiation-induced gaseous ions in the surrounding atmosphere. The CNT FET devices were fabricated as reported elsewhere in the literature [42, 61, 62]. Fig. 6 illustrates the device layout.

The 88-Inch Cyclotron was used to direct 50 MeV protons and 10 MeV/Nucleon Xe ions onto the samples, while the electrical properties of the devices were characterized in-situ with an Agilent 4155 semiconductor parameter analyzer. The average proton flux during these measurements was $1.5x10^8$ protons/cm^2/s. Fig. 7 shows a picture of the experimental setup.

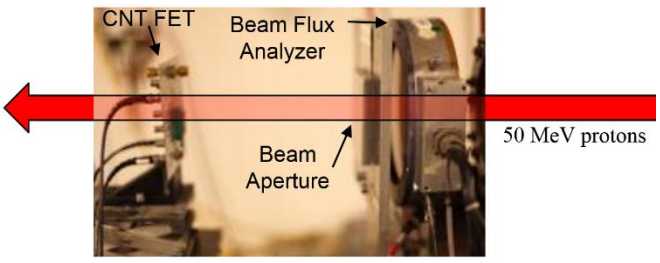

Fig. 7. Picture of the experimental setup. The proton beam was passed through a beam aperture and directed onto the sample in air. CNT FET devices were electrically characterized in-situ, during radiation exposure.

Fig. 8 plots the drain current versus gate voltage for the CNT FET before and after exposure to $2x10^{12}$ protons/cm^2, which gives an equivalent dose of 326 krad(Si). After exposure to the proton radiation, there is a positive threshold voltage shift of less than 200 mV. This is attributed to negative charge traps in the underlying SiN_x on the edges of the trench (100 nm thickness). The suspended nature of these devices results in minimal gate-dielectric TID effects.

Fig. 9 plots the drain current versus time for a CNT FET during exposure to proton radiation, showing the observed TREs, which is attributed to interaction of ionized gas molecules in the surrounding atmosphere interacting with the device. These data are characteristic of the devices that showed such TREs, where the device current is reduced substantially, sometimes by over two orders of magnitude. The source-drain voltage applied to the device was 0.1 V, and the gate voltage was held at 0 V. The average duration of ion residency varies greatly, from as low as 8 ms (instrument limited) to many hours.

The ability of a single charge to cause large changes in conductance in a single carbon nanotube device is rooted in the one-dimensional nature of electrical transport in CNTs. Charge carriers are not free to route around scattering sites or potential barriers, and the conductance of the entire device is compromised, giving rise to the large changes in conductance. The ramifications of these measurements are that as electronic devices are scaled down to nanometer dimensions, they may become increasingly sensitive to radiation induced switching or charging of individual defects in sensitive areas. Understanding these defects may therefore be a key step in developing nano-electronics for use in the space environment. Further details of this work are published elsewhere [63, 64].

V. Conclusions

In the upper layers of the atmosphere and in outer space, radiation constitutes a serious problem for the aerospace electronics.

When high-energy ions enter a material, they lose most of the energy at the Bragg peak. As a result, an energy variable accelerator can be used to regulate the depth and amount of energy deposited to systematically test electronics parts in a controlled manner.

The combination of the 88-Inch Cyclotron with the ECR ion sources makes a unique apparatus that allows switching ion species and energies in minutes. Currently, it produces 2000 hours per year of heavy and light ions, neutrons, and microbeams devoted to study transient and long lasting effects of ions impacting electronics.

As the electronics structures and devices are constantly scaled to smaller sizes, the effects of radiation become increasingly more important. Experimental measurements of the neutron spectra from thick target deuteron breakups demonstrate the advantages of the high-flux tunable spectrum

neutron beam produced at the 88-Inch Cyclotron compared to the LANSCE/WNR Facility and illuminate opportunities for neutron damages studies.

New technologies, such as the Carbon nanotube field effect transistor, were tested in a radiation controlled environment to understand its performance and degradation mechanisms in the presence of radiation.

The 88-Inch Cyclotron can simulate the space environment conditions that the electronics will be exposed over the years in matter of minutes. It constitutes an essential tool to develop radiation-hardened circuits and design techniques to avoid very costly loss of equipment from the aerospace industry.

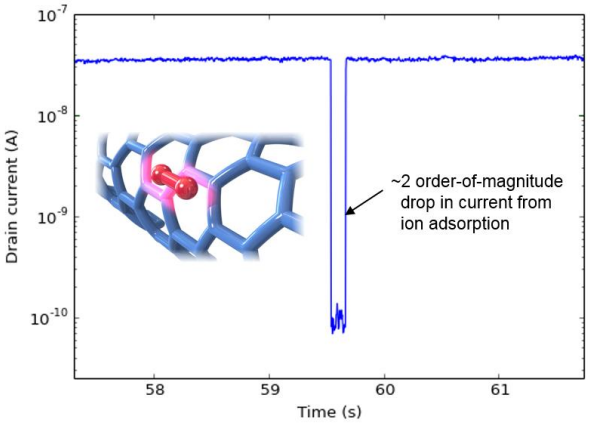

Fig. 9. Drain current versus time during single-gaseous ion adsorption event and subsequent desorption a fraction of a second later. Inset shows a cartoon depiction of an ionized nitrogen molecule on the surface of a CNT.

ACKNOWLEDGMENT

The authors want to thank Craig F. Rogers, Brendan P. Cronander-Ford, Robert J. Ramer, and Mark Regis for the electronics support; Catherine R. Siero, Thomas L. Gimpel, Scott M. Small, Sierra Garret, and Nicholas M. Brickner for the operation support; John P. Garcia, Donald Bell, and Brian D. Reynolds for the mechanical support; and Rocky Koga, Steve Bielat, and Jeffrey George for assistance with operation of the LBNL 88-Inch Cyclotron. The authors also acknowledge Steve Moss, Ron Lacoe, Cory Cress and Jon Osborn for helpful discussions regarding interpretation of the data.

REFERENCES

[1] J. L. Burch, “The fury of space storms,” Scientific American 2001; 284(4):86-94.

[2] D. F. Smart and M.A. Shea, “Solar radiation,” In Encyclopedia of applied physics, vol. 18. New York, NY: VCH Publishers, 1997: 393-429.

[3] J. S. Mayo, H. Mann, F. J. Witt, D. S. Peck, H. K. Gummel, and W. L. Brown, “The command system malfunction of the Telstar satellite,” NASA SP-32, Vol. 2, (1963), 1631-1657.

[4] M. Kireeff Covo, A. W. Molvik, A. Friedman, G. Westenskow, J. J. Barnard, R. Cohen, P. A. Seidl, J. W. Kwan, G. Logan, D. Baca, F. Bieniosek, C. M. Celata, J. L. Vay, and J. L. Vujic, “Beam energy scaling of ion-induced electron yield from K+ impact on stainless steel,” Phys. Rev. ST Accel. Beams 9, 063201 (2006).

[5] F. B. McLean and T. R. Oldham, "Charge funneling in n- and p-type substrates," IEEE Trans. Nucl. Sci., NS-29, 2018 (1982).

[6] K. LaBel, M. Gates, J. Barth, A. Johnston and P. Marshall, “Single event effect criticality analysis (SEECA),” Sponsored by NASA Headquarters/Code QW, http://radhome.gsfc.nasa.gov/radhome/papers/seecai.htm, Feb 15, 1996.

[7] M. A. McMahan, “Radiation effects testing at the 88-Inch Cyclotron,” In Proceedings of the Fifth European Conference on Radiation and Its Effects on Components and Systems, RADECS 99, USA (1999), p.142, doi: 10.1109/RADECS.1999.858563.

[8] G. D. Alton and D. N. Smithe, “Design studies for an advanced ECR ion source,” Rev. Sci. Instrum., vol. 65, no. 4, pp. 775–787, Apr. 1994.

[9] R. Geller, F. Bourg, P. Briand, J. Debernardi, M. Delaunay, B. Jacquot, P. Ludwig, R. Pauthenet (in memoriam), M. Pontonnier, and P. Sortais, “The Grenoble ECRIS status 1987 and proposals for ECRIS scalings,” in Proc. 8th Workshop ECRIS, East Lansing, MI, 1987, p. 1.

[10] C. M. Lyneis, Z. Q. Xie, D. J. Clarck, R. S. Lam, and S. A. Lundgren, “Preliminary performance of the LBL AECR,” In Proceedings of 10th International Workshop on ECR Ion Sources, Oak Ridge, TN, USA, 1990, 47.

[11] M. Kireeff Covo, J. Y. Benitez, A. Ratti, and J. L. Vujic, “Integrating a traveling wave tube into an AECR-U ion source,” IEEE Trans. on Plasma Sci. 39 (2011) 1455, DOI: 10.1109/TPS.2011.2130542.

[12] C. M. Lyneis, Z. Q. Xie, and C. E. Taylor, “Design of the 3rd generation ECR ion source,” In Proceedings of the 13th International Workshop on ECR Ion Sources, Texas A&M University, USA, 1997, 115.

[13] D.Z. Xie, J.Y. Benitez, A. Hodgkinson, T. Loew, C.M. Lyneis, L. Phair, P. Pipersky, B. Reynolds, and D. S. Todd. “Development status of a next generation ECRIS: MARS-D at LBNL,” Rev. Scient. Instr. 87 (2016) 02A702, DOI: http://dx.doi.org/10.1063/1.4931713.

[14] B. G. Harvey, Nuclear Spectroscopy and Reactions, Part A, Academic Press Inc., New York, 1974.

[15] D. Leitner, M. A. McMahan, D. Argento, T. Gimpel, A. Guy, J. Morel, C. Siero, R. Thatcher, C. M. Lyneis, “Heavy ion cocktail beams at the 88 Inch Cyclotron,” Report LBNL-51451, 2002.

[16] M. Kireeff Covo, “Measurement of axial injection displacement with trim coil current unbalance,” Rev. Scient. Instr. 85 (2014) 085113, DOI: http://dx.doi.org/10.1063/1.4892463.

[17] M. Kireeff Covo, “Nondestructive synchronous beam current monitor,” Rev. Scient. Instr. 85 (2014) 125106, DOI: http://dx.doi.org/10.1063/1.4902903.

[18] http://gretina.lbl.gov/

[19] K. E. Gregorich, “Simulation of recoil trajectories in gas-filled magnetic separators,” Nucl. Instr. Meth. A711, 47 (2013)

[20] J. M. Gates, “Prospects of A and Z identification experiments at LBNL,” Nobel Symposium NS 160 - Chemistry and Physics of Heavy and Superheavy Elements, Bäckaskog Castle, Sweden, Edited by Rudolph, D.; EPJ Web of Conferences, Volume 131, id.0800, December 2016, DOI: 10.1051/epjconf/201613108003

[21] M. A. McMahan, L. Ahle, D.L. Bleuel, L. Bernstein, B.R. Barquest, J. Cerny, L.H. Heilbronn, C.C. Jewett, I. Thompson, and B. Wilson, “Neutron beams from deuteron breakup at the 88-Inch Cyclotron at Lawrence Berkeley National Laboratory,” ND2007, 411-414 (2007), DOI: 10.1051/ndata:07456

[22] D. L. Bleuel, M. A. McMahan, L. Ahle, B. R. Barquest, J. Cerny, L. H. Heilbronn, and C.C. Jewett, “Characterization of a tunable quasi-monoenergetic neutron beam from deuteron breakup,” Nuclear Instruments and Methods in Physics Research Section B: Beam Interactions with Materials and Atoms, Volume 261, Issues 1–2, August 2007, Pages 974-979, ISSN 0168-583X, http://dx.doi.org/10.1016/j.nimb.2007.04.125.\

[23] G.W. Schweimer, “Fast neutron production with 54 MeV deuterons,” Nucl. Phys., A 100, 537 (1969).

[24] J. P. Meulders, P. Leleux, P. C. Macq and C. Pirart, Phys. Med. Biol., 1975, Vol.. 20, No. 2, 235-243. (1975).

[25] J.A. Brown et al., J. Appl. Phys. 115, 193504 (2014).

[26] R. Beyer, R. Schwengner, R. Hannaske, A.R. Junghans, R. Massarczyk, M. Anders, D. Bemmerer, A. Ferrari, A. Hartmann, T. Kögler M. Röder, K. Schmidt, and A. Wagner, "Inelastic scattering of fast neutrons from excited states in ^{56}Fe," Nucl. Phys. A 927 (2014) 41-52

[27] A. Negret, C. Borcea, Ph. Dessagne, M. Kerveno, A. Olacel, A.J.M. Plompen, and M. Stanoiu, "Cross-section measurements for the ^{56}Fe(n,xnγ) reactions," PRC 90, 034602 (2014)

[28] http://www.micro-rdc.com/SEE%20Testing.htm

[29] S. Ritt, P. Amaudruz, The MIDAS DAQ System, in: Proceedings of the 10th IEEE Real Time Conference, Beaune (1997) 309. http://midas.triumf.ca

[30] R.Brun and F.Rademakers, ROOT - An object oriented data analysis framework, Nucl. Instrum. Meth. A, 389 (1997) 81-86.

[31] M. Matzke, HEPROW, Unfolding of pulse height spectra using Bayes theorem and maximum entropy method, Organisation for Economic Co-Operation and Development, Nuclear Energy Agency, NEA1666/01, 2004.

[32] S. Agostinelli, GEANT4 - a simulation toolkit, Nucl. Instrum. Meth. A, 506 (2003) 250-303.

[33] G.Dietze and H.Klein, Gamma-calibration of NE 213 scintillation counters, Nucl. Instrum. Meth. in Phys. Res., 193 (1982) 549-556.

[34] J.A. Brown *et al.*, "Relative light yield and temporal response of a stilbene-doped bibenzyl organic scintillator for neutron detection". J. Appl. Phys 115, 193504 (2014).

[35] T. Durkop, S. A. Getty, E. Cobas, and M. S. Fuhrer, "Extraordinary Mobility in Semiconducting Carbon Nanotubes," *Nano Lett.*, vol. 4, pp. 35-39, 2004.

[36] J. Baumgardner, A. Pesetski, J. Murduck, J. Przybysz, J. Adam, and H. Zhang, "Inherent linearity in carbon nanotube field-effect transistors," *Applied Physics Letters*, vol. 91, p. 052107, 2007.

[37] J. Li, Y. J. Lu, Q. Ye, M. Cinke, J. Han, and M. Meyyappan, "Carbon nanotube sensors for gas and organic vapor detection," *Nano Letters*, vol. 3, pp. 929-933, Jul 2003.

[38] V. Sazonova, Y. Yaish, H. Ustünel, D. Roundy, T. A. Arias, and P. L. McEuen, "A tunable carbon nanotube electromechanical oscillator," *Nature*, vol. 431, p. 284, 2004.

[39] D.-m. Sun, M. Y. Timmermans, Y. Tian, A. G. Nasibulin, E. I. Kauppinen, S. Kishimoto, *et al.*, "Flexible high-performance carbon nanotube integrated circuits," *Nature Nanotechnology*, vol. 6, pp. 156-161, 2011.

[40] P. J. Burke, "AC performance of nanoelectronics: towards a ballistic THz nanotube transistor," *Solid-State Electronics*, vol. 48, pp. 1981-1986, 2004.

[41] Z. Yao, C. L. Kane, and C. Dekker, "High-Field Electrical Transport in Single-Wall Carbon Nanotubes," *Physical Review Letters*, vol. 84, p. 2941, Mar. 2000.

[42] E. Pop, D. Mann, J. Cao, Q. Wang, K. Goodson, and H. Dai, "Negative differential conductance and hot phonons in suspended nanotube molecular wires," *Physical Review Letters*, vol. 95, pp. 155505-8, Oct. 2005.

[43] M. Lazzeri, S. Piscanec, F. Mauri, A. C. Ferrari, and J. Robertson, "Electron Transport and Hot Phonons in Carbon Nanotubes," *Physical Review Letters*, vol. 95, pp. 236802-5, Nov. 2005.

[44] J. Kong, E. Yenilmez, T. W. Tombler, W. Kim, H. Dai, R. B. Laughlin, *et al.*, "Quantum Interference and Ballistic Transmission in Nanotube Electron Waveguides," *Physical Review Letters*, vol. 87, p. 106801, 2001.

[45] V. V. Deshpande and M. Bockrath, "The one-dimensional Wigner crystal in carbon nanotubes," *Nat Phys*, vol. 4, pp. 314-318, Mar. 2008.

[46] M. Bockrath, D. H. Cobden, J. Lu, P. L. McEuen, A. G. Rinzler, R. E. Smalley, *et al.*, "Luttinger-liquid behaviour in carbon nanotubes," *Nature*, vol. 397, pp. 598-601, 1999.

[47] B. Dora, M. Gulacsi, F. Simon, and H. Kuzmany, "Spin Gap and Luttinger Liquid Description of the NMR Relaxation in Carbon Nanotubes," *Physical Review Letters*, vol. 99, pp. 166402-4, 2007.

[48] H. Ishii, H. Kataura, H. Shiozawa, H. Yoshioka, H. Otsubo, Y. Takayama, *et al.*, "Direct observation of Tomonaga-Luttinger-liquid state in carbon nanotubes at low temperatures," *Nature*, vol. 426, pp. 540-544, 2003.

[49] C. Cress, J. McMorrow, J. Robinson, A. Friedman, H. Hughes, B. Weaver, *et al.*, "Total ionizing dose-hardened carbon nanotube thin-film transistors with silicon oxynitride gate dielectrics," *MRS Commun.*, vol. 1, pp. 27-31, 2011.

[50] C. D. Cress, J. J. McMorrow, J. T. Robinson, A. L. Friedman, and B. J. Landi, "Radiation Effects in Single-Walled Carbon Nanotube Thin-Film-Transistors," *IEEE Trans. Nucl. Sci.*, vol. 57, pp. 3040-3045, 2010.

[51] E. S. Comfort, M. Fishman, A. Malapanis, H. Hughes, P. McMarr, C. D. Cress, *et al.*, "Creation of Individual Defects at Extremely High Proton Fluences in Carbon Nanotube p-n Diodes," *IEEE Trans. Nucl. Sci.*, vol. 58, pp. 2898-2903, 2011.

[52] C. D. Cress, J. J. McMorrow, J. T. Robinson, B. J. Landi, S. M. Hubbard, and S. R. Messenger, "Radiation effects in carbon nanoelectronics," *Electronics*, vol. 1, pp. 23-31, 2012.

[53] F. Liu, K. L. Wang, C. Li, and C. Zhou, "Study of random telegraph signals in single-walled carbon nanotube field effect transistors," *IEEE Trans. Nanotechnol.*, vol. 5, pp. 441-445, 2006.

[54] F. Liu, K. L. Wang, D. Zhang, and C. Zhou, "Noise in carbon nanotube field effect transistor," *Applied Physics Letters*, vol. 89, p. 063116, 2006.

[55] B. R. Goldsmith, J. G. Coroneus, A. A. Kane, G. A. Weiss, and P. G. Collins, "Monitoring Single-Molecule Reactivity on a Carbon Nanotube," *Nano Letters*, vol. 8, pp. 189-194, 2007.

[56] B. R. Goldsmith, J. G. Coroneus, V. R. Khalap, A. A. Kane, G. A. Weiss, and P. G. Collins, "Conductance-Controlled Point Functionalization of Single-Walled Carbon Nanotubes," *Science*, vol. 315, pp. 77-81, Jan. 2007.

[57] Z. J. Donhauser, B. A. Mantooth, K. F. Kelly, L. A. Bumm, J. D. Monnell, J. J. Stapleton, *et al.*, "Conductance Switching in Single Molecules Through Conformational Changes," *Science*, vol. 292, pp. 2303-2307, Jun. 2001.

[58] K. K. Hung, P. K. Ko, C. Hu, and Y. C. Cheng, "Random telegraph noise of deep-submicrometer MOSFETs," *IEEE electron device letters*, vol. 11, pp. 90-92, 1990.

[59] K. S. Ralls, W. J. Skocpol, L. D. Jackel, R. E. Howard, L. A. Fetter, R. W. Epworth, *et al.*, "Discrete Resistance Switching in Submicrometer Silicon Inversion Layers: Individual Interface Traps and Low-Frequency 1/f Noise," *Physical Review Letters*, vol. 52, pp. 228-231, 1984.

[60] M. J. Uren, D. J. Day, and M. J. Kirton, "1/f and random telegraph noise in silicon metal-oxide-semiconductor field-effect transistors," *Applied Physics Letters*, vol. 47, pp. 1195-1197, 1985.

[61] A. W. Bushmaker, V. V. Deshpande, S. Hsieh, M. W. Bockrath, and S. B. Cronin, "Gate Voltage Controllable Non-Equilibrium and Non-Ohmic Behavior in Suspended Carbon Nanotubes," *Nano Letters*, vol. 9, pp. 2862-2866, Jul. 2009.

[62] J. Cao, Q. Wang, and H. Dai, "Electron transport in very clean, as-grown suspended carbon nanotubes," *Nature Materials*, vol. 4, pp. 745-749, 2005.

[63] A. W. Bushmaker, D. Walker, C. J. Mann, V. Oklejas, A. R. Hopkins, M. R. Amer, *et al.*, "Single Event Effects in Carbon Nanotube-Based Field Effect Transistors Under Energetic Particle Radiation," *IEEE Trans. Nucl. Sci.*, vol. 61, p. 2839, 2014.

[64] A. W. Bushmaker, V. Oklejas, D. Walker, A. R. Hopkins, J. Chen, and S. B. Cronin, "Single-ion adsorption and switching in carbon nanotubes," *Nat Commun*, vol. 7, 2016.

Table 1. 4.5, 10, 16 and 30 AMeV ion cocktails.

Ion	Cocktail (AMeV)	Energy (MeV)	Z	A	Chg. State	% Nat. Abund.	LET 0° $\left(\frac{MeV}{mg.cm^2}\right)$	Range (μm)
B	**4.5**	44.90	5	10	+2	2.0E+01	**1.65**	78.5
N	**4.5**	67.44	7	15	+3	3.7E-01	**3.08**	67.8
Ne	**4.5**	89.95	10	20	+4	9.0E+01	**5.77**	53.1
Si	**4.5**	139.61	14	29	+6	4.7E+00	**9.28**	52.4
Ar	**4.5**	180.00	18	40	+8	1.0E+02	**14.32**	48.3
V	**4.5**	221.00	23	51	+10	1.0E+02	**21.68**	42.5
Cu	**4.5**	301.79	29	63	+13	6.9E+01	**29.33**	45.6
Kr	**4.5**	378.11	36	86	+17	1.7E+01	**39.25**	42.4
Y	**4.5**	409.58	39	89	+18	1.0E+02	**45.58**	45.8
Ag	**4.5**	499.50	47	109	+22	4.8E+01	**58.18**	46.3
Xe	**4.5**	602.90	54	136	+27	8.9E+00	**68.84**	48.3
Tb	**4.5**	724.17	65	159	+32	1.0E+02	**77.52**	52.4
Ta	**4.5**	805.02	73	181	+36	1.0E+02	**87.15**	53.0
Bi*	**4.5**	904.16	83	209	+41	1.0E+02	**99.74**	52.9
B	**10**	108.01	5	11	+3	8.0E+01	**0.89**	305.7
O	**10**	183.47	8	18	+5	2.0E-01	**2.19**	226.4
Ne	**10**	216.28	10	22	+6	9.3E+00	**3.49**	174.6
Si	**10**	291.77	14	29	+8	4.7E+00	**6.09**	141.7
Ar	**10**	400.00	18	40	+11	1.0E+02	**9.74**	130.1
V	**10**	508.27	23	51	+14	1.0E+02	**14.59**	113.4
Cu	**10**	659.19	29	65	+18	3.1E+01	**21.17**	108.0
Kr	**10**	885.59	36	86	+24	1.7E+01	**30.86**	109.9
Y	**10**	928.49	39	89	+25	1.0E+02	**34.73**	102.2
Ag	**10**	1039.42	47	107	+29	5.2E+01	**48.15**	90.0
Xe	**10**	1232.55	54	124	+34	1.0E-01	**58.78**	90.0
Au*	**10**	1955.87	79	197	+54	1.0E+02	**85.76**	105.9
He*	**16**	43.46	2	3	+1	1.3E-04	**0.11**	1020.0
N	**16**	233.75	7	14	+5	1.0E+02	**1.16**	505.9
O	**16**	277.33	8	17	+6	4.0E-02	**1.54**	462.4
Ne	**16**	321.00	10	20	+7	9.0E+01	**2.39**	347.9
Si	**16**	452.10	14	29	+10	4.7E+00	**4.56**	274.3
Cl	**16**	539.51	17	35	+12	7.6E+01	**6.61**	233.6
Ar	**16**	642.36	18	40	+14	1.0E+02	**7.27**	255.6
V	**16**	832.84	23	51	+18	1.0E+02	**10.90**	225.8
Cu	**16**	1007.34	29	63	+22	6.9E+01	**16.53**	190.3
Kr	**16**	1225.54	36	78	+27	3.5E-01	**24.98**	165.4
Xe*	**16**	1954.71	54	124	+43	1.0E-01	**49.29**	147.9
N	**30**	425.45	7	15	+7	3.7E-01	**0.76**	1370.0
O	**30**	490.22	8	17	+8	4.0E-02	**0.98**	1220.0
Ne	**30**	620.00	10	21	+10	2.7E-01	**1.48**	1040.0
Ar	**30**	1046.11	18	36	+17	3.4E-01	**4.87**	578.1